Interpretation on Breast Cancer Image Data Received form Ultrasonography, Mammography and Magnetic Resonance

Madhavi Pingili[1*], Prof. E G Rajan[2]

[1*]Research Scholar, Dept of Computer Science, MG-NIRSA, University of Mysore, India.

[2]Director, MG-NIRSA, University of Mysore, India.

Abstract

In real time the Sonographer can do scanning, analyze, and describe to the best of accuracy dependent on their own insight. Here breast images are taken for research examination. Ultrasonography is an instrument used for breast imaging, where the sonographer makes some ongoing comprehension of the patient's breast malignant growth status. Breast malignancy investigation is generally completed on scanned images, which are acquired utilizing either sonographic or mammographic imaging frameworks. Clamor evacuation methods must be utilized for expulsion of errors in the scanned images for better reports. For future investigation, the scanning strategy can be carefully recorded as a video or stills. In opposition to this strategy, one can also choose mammographic x-ray beam imaging and progressed radiological methods to get away from images of patient's breast with the end goal of finding.

Keywords:Breast Cancer, Ductal carcinoma, Mammographic, Ultra-Sonographic, Clamor

Introduction

In this serious world, medical services experts and researchers maintaining their high spotlight on one of the two significant issues, (i) Ductal carcinoma in situ (DCIS) and (ii) Invasive ductal carcinoma (IDC). In General, Radiologists analyze visually the mammographic or MR images with the assistance of image investigation supportive network built in the scanning devices. Ultra-sonographic breast disease images are considered for this research. These sorts of images are regularly used to control breast biopsies. Ultra-sonographic imaging is discovered to be an amazingly valuable method, particularly for ladies with thick breast and a negative mammogram. However, they end up in ‘false negative’ and ‘false positive’ choices, which represent an issue of worry as on date.

This paper attempts to give a fundamental achievable answer for this issue. Gamma Correction formula is utilized to tackle this issue. This equation is a transformation of linear luminance-based images into a nonlinear luminance-basedimages. Breast cancer detection in a mammography image before a lump appears or some other symptoms show up usually leads to the conclusion that mammogram has done a fine job. Shockingly, the vast majority of the patients don't profit by the examination of mammography images not on the grounds that mammography isn't right, but because of the absence of solid image handling and pattern recognition and translation strategies.

Generally, a screening assessment doesn't yield a complete outcome. The patients who don't experience the ill effects of malignant growth yet are exposed to additional testing separated from mammographic scanning are alluded to as "false positives". This implies that false positive mammograms influence ladies normal behavior and prosperity. Despite the fact that false positive ladies go through routine screening or perform self-assessments, some of them become restless and expect that they have breast malignancy. It is an undesirable and more so tedious cycle for both false positives and diagnostic centers to get into regular screening strategies. Now and then, false positive outcomes end up being over symptomatic. To add to additional uneasiness, mammograms by and large do not show up tumors for unaided eyes of a radiologist thus ladies are pointlessly arranged as "false negatives."

Filters for Removing Clamor in Ultrasonography Image

Ultrasonography Image: A strategy that utilizes high-energy sound waves to take a gander at tissues and organs inside the body. The sound waves make echoes that structure photos of the tissues and organs on a PC screen (sonogram). Ultrasonography might be utilized to help analyze illnesses, for example, malignant growth and so on. This is a procedure and operator dependent and the sonographer or a radiologist must have high experience in scanning. For analysis past reports and continuous process of scanning is also helpful. Following images Fig. 1 and Fig. 2 shows the cancer mass present in the breast. Fig.1 is not seen clearly on IDC. If the scanning is done again it is clearly seen in Fig. 2. This is a painless procedure, and the perception is clear if the checked images are in shading. Target examining is done for ladies having exceptionally little breast with transducers working on 17 MHz f. The most basic issue presented by ultrasonography image is 'spot clamor', which makes symptomatic cycle difficult. So appropriate filters are to be utilized for denoising. Spot clamor debases the nature of images and better subtleties of the body parts are not seen appropriately. This commotion limits contrast goal with the end goal that low difference sores in the scanned image are not appropriately envisioned.

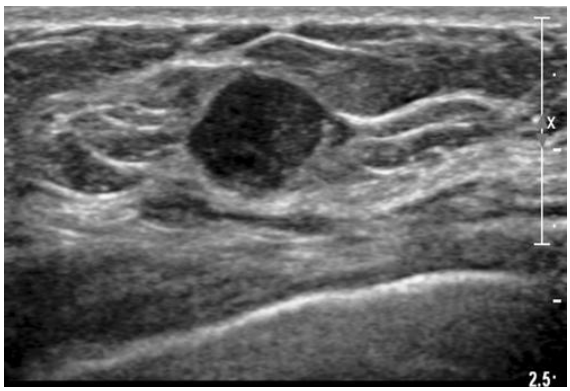

Targeted gray-scale ultra-sonographic image showing 1.4-cm solid hypoechoic mass

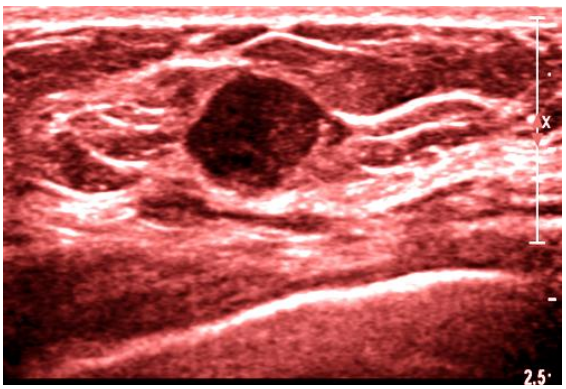

Color version of targeted ultra-sonographic image
showing 1.4-cm solid hypoechoic mass

Fig. 1: Ultra-sonographic targeted image and its colored version

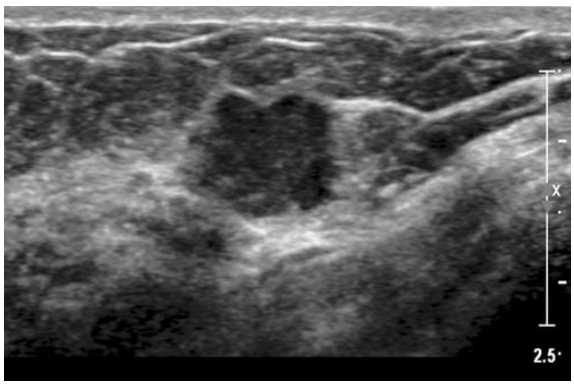

Repeat ultra-sonographic image scanned through the
entire mass, which shows an invasive ductal carcinoma

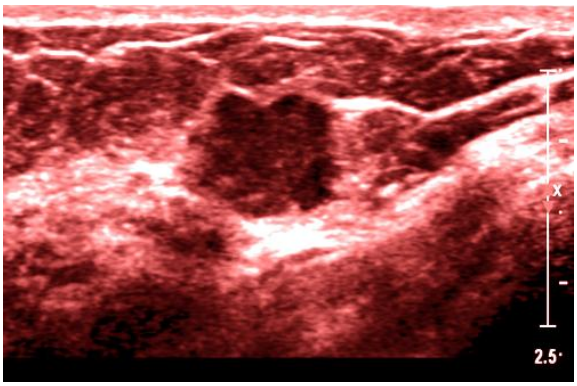

Color version of repeat ultra-sonographic image scanned through the entire mass, which shows an invasive ductal carcinoma

Fig. 2: Ultra-sonographic targeted image and its colored version – a repeated scan

Clamor/Speckle Noise removing with filters

Speckle noise is the clamor that emerges because of the impact of ecological conditions on the imaging sensor during image obtaining. Speckle noise is generally recognized in the event of clinical images. The large test in ultrasound imaging is denoising, this explanation is being the presence of speckle artifacts. Making a numerical model is somewhat hard for it since this sort of speckle noise is tissue based. Various tissues show distinctive acoustic impedances and the ultrasound frequency waves sent by the imaging framework is halfway reflected and generally communicated by the tissue limits.

Lessening speckle artifacts should be possible by an elevated level plan of the filter. Numerous algorithms are proposed so far for eliminating Speckle clamor in ultrasound images are unfriendly for visual. Utilization of higher frequencies would yield better image goal however will restrict profundity of entrance. Consequently, one needs to pick fitting ultrasonic frequency according to requirement. Alternatively, speckle artifacts evacuation procedures dependent on logarithmic methodology may yield better outcomes. To have an unmistakable comprehension beneath approaches used.
For reducing or removing speckle noise, algorithms which use logarithmic transformations and nonlinear estimations will give better results without damaging quality and morphology of image features at the time of visualization. 2D- autocorrelation method is most preferred procedure for white noise removing.

2D autocorrelation: Noise removing

Noise removal using 2D autocorrelation

In general, 2D autocorrelation is basically a pixel value intensifier and not commotion remover. On the other hand, Gaussian filter is a commotion remover. In this way, autocorrelation of a Gaussian separated image would yield power improved denoised image. Autocorrelation is a function by itself. In numerical terms, autocorrelation is determined as

$$Gii(a,b) = \sum_{x}^{M}\sum_{y}^{N} i(x,y) * i(x-a, y-b)$$

- Autocorrelation function is *Gii(a,b)*
- Image pixel intensity at *(x,y)* is *i(x,y)*
- Distance from (*x, y)* represented by *a,b.*
- *Width* and height of the image are represented by *M, N.*

This equation is a mathematical model for autocorrelating similar images which are equal in nature. Now the normalized autocorrelation is defined by the equation given below:

$$gii(a,b) = \frac{\sum_{x}^{M}\sum_{y}^{N} i(x,y) * i(x-a, y-b)}{\sum_{x}^{M}\sum_{y}^{N} i(x,y) * i(x,y)} - 1 = \frac{F^{-1}\{F[i(x,y)]^2\}}{NMi^2} - 1$$

The autocorrelation of Gaussian is another Gaussian function with smaller standard deviations. For instance, consider a digital x-ray chest image shown in Fig. 3(a). Fig. 3(b) shows its Gaussian filtered version.

(a) Original image with noise (b) Gaussian filtered image of (a) (c) Autocorrelated version of image (b)

Fig. 3: Noise removal using autocorrelation of Gaussian filtered image

Fig. 3(c) shows the autocorrelated version of the Gaussian filtered image of Fig. 3(b). Gaussian filtered image shown in Fig. 3(b) could be seen to be almost free of speckle noise and image shown in Fig. 3(c) to be intensity enhanced.

Optimized Bayesian Non Local Means (OBNLM) filter for Noise removal

OBNLM method is mostly used to remove speckle noise in an ultrasound image using a Bayesian motivation for the Non-Local Means filtering. In this case, the signal at a pixel is modeled as a zero mean Gaussian random variable with a variance determined by the scattering properties of the scanned tissue at the current pixel. OBNLM algorithm is commonly used for processing ultrasound images.

The theoretical connections to diffusion and non-parametric estimation of a neighborhood filter is basically NL-means filter. It is defined as

$$NL\,z(x) = \frac{1}{C(x)} \sum_{y \in \Omega} w(x,y)\, z(y)$$

,

$z = (z(x))_{x \in \Omega}$ is the input image at region $\Omega \subset \mathbb{R}^2$,

Nnoisy image pixel is *z(x)*

Average weighted pixel values is NL Z(x)

Normalizing values can be obtained by $C(x) = \sum_{y \in \Omega} w(x,y)$, *w(x,y)* are the weights computed using the equation:

$$w(x,y) = \exp\left(-\frac{1}{h^2}\int_{\mathbb{R}^2} G_a(t)|z(x+t)-z(y+t)|^2 dt\right) := \exp\left(-\frac{\|\mathbf{z}(x)-\mathbf{z}(y)\|^2_{2,a}}{h^2}\right)$$

h is approximately equal to 12σ, *G(t)* is the Gaussian kernel with standard deviation that decides the distance between the central pixel under the scanning window and other pixels

Log Normal Filtering (LN) Algorithm

$z(i, j) = \{[W \log(a(i, j)) / \log(W)]^n\} / W^{n-1}$

The above equation is for Log Normal algorithm

where *z(i, j)* is the output pixel value, *a(i, j)* is the OBNLM filtered input image pixel value, *W* is the maximum intensity value present in the OBNLM filtered image and n is a constant. Fig. 4 shows the LN filter characteristics with various values for n.

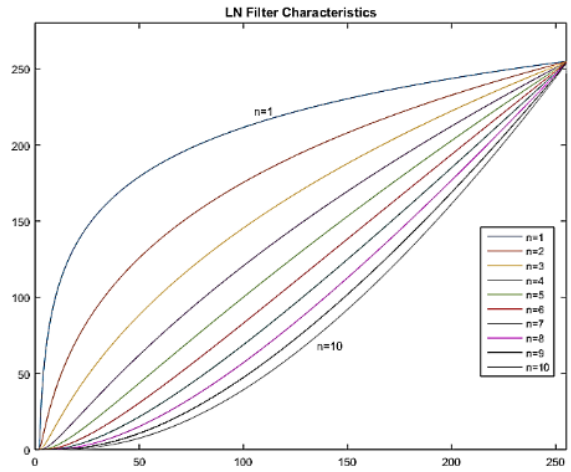

Fig. 4: Filter characteristics of LN filter

Hybridization of OBNLM and LN filters

Fig. 5 is ***Hybridization of OBNLM and LN filters which*** shows a breast image, its logarithmic version and normalized version followed by OBNLM filtering.

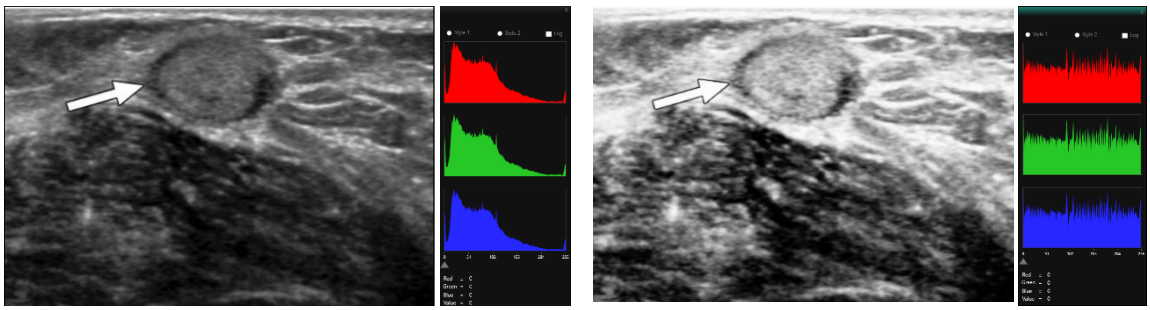

Ultrasonographic breast image | Histogram | Gamma and OBNLM filtered image | Histogram

Fig. 5: Sample breast cancer image, its OBNLM filtered version and histograms

With reference to Fig. 5, one may observe that despeckling of ultrasonography breast image is essential to visualize most of the hidden information due to presence of noise.

Statistics and Visual Quality Measures

The statistics of the ultrasonography images shown in Fig. 5 before and after OBNLM filtering are given in table 1.

Table 1: Statistics of sample image before and after OBNLM filtering

Statistics of ultrasonographic breast image with speckle noise		Statistics of ultrasonographic breast image after OBNLM filtering	
Pixels Count	175044	Pixels Count	173153
Pixels without black	173865	Pixels without black	171939
Red Min	0	Red Min	0
Red Max	255	Red Max	253
Red Mean	73.2685667603574	Red Mean	126.068367282115
Red Standard Deviation	48.2617100479182	Red Standard Deviation	73.0906383910361
Red Median	67	Red Median	126
Red Total Count	175044	Red Total Count	173153
Green Min	0	Green Min	0
Green Max	255	Green Max	253
Green Mean	73.2685667603574	Green Mean	126.068367282115
Green Standard Deviation	48.2617100479182	Green Standard Deviation	73.0906383910361
Green Median	67	Green Median	126
Green Total Count	175044	Green Total Count	173153
Blue Min	0	Blue Min	0
Blue Max	255	Blue Max	253
Blue Mean	73.2685667603574	Blue Mean	126.068367282115
Blue Standard Deviation	48.2617100479182	Blue Standard Deviation	73.0906383910361
Blue Median	67	Blue Median	126
Blue Total Count	175044	Blue Total Count	173153

Fig. 6: Mean values of Red, Green and Blue components before and after filtering

From Table.1 and Fig. 6, one can see that the mean estimations of Red, Green and Blue segments of the filtered image is practically 1.5 times (on a normal) more than those of the first scanned image. The separating activity proposed in this paper yields a sort of evened out yield yet with the expulsion of speckle noise, and subsequently the method is prescribed to be utilized for preprocessing ultrasonography breast image for malignant growth study.

Visual quality measures

An experiment has been performed on the scanned image given in Fig. 5 and the observations presented in Table 2. Relationship between entropy and visual quality of scanned image is given in Fig. 7

Table 2: Visual quality measures of scanned breast image

Visual Quality, Trade of Threshold and Human Visual Quantization Threshold of ultrasonographic breast image							
Threshold	Counter	Image Size	Visual Quality	Entropy	|Entropy-Visual Quality|	ToT	HVQT
0	0	175044	0	100	100		
1	101	175044	0.057699778	99.94230022	99.88460044		
2	681	175044	0.38904504	99.61095496	99.22190992		
3	2191	175044	1.251685291	98.74831471	97.49662942		
4	5341	175044	3.051232833	96.94876717	93.89753433		
5	10592	175044	6.051050022	93.94894998	87.89789996		
6	17417	175044	9.950069697	90.0499303	80.09986061		
7	25515	175044	14.57633509	85.42366491	70.84732981		
8	34363	175044	19.63106419	80.36893581	60.73787162		
9	43523	175044	24.86403419	75.13596581	50.27193163		
10	52709	175044	30.11185759	69.88814241	39.77628482		
11	61736	175044	35.26884669	64.73115331	29.46230662		
12	70370	175044	40.20132081	59.79867919	19.59735838		
13	78403	175044	44.79045269	55.20954731	10.41909463		
14	85979	175044	49.11850735	50.88149265	1.762985307	14	
15	92909	175044	53.07751194	46.92248806	6.15502388		
16	99372	175044	56.76972647	43.23027353	13.53945294		
17	105361	175044	60.19115194	39.80884806	20.38230388		
18	110925	175044	63.36978131	36.63021869	26.73956262		
19	115955	175044	66.24334453	33.75665547	32.48668906		
20	120508	175044	68.84440484	31.15559516	37.68880967		
21	124592	175044	71.17753251	28.82246749	42.35506501		
22	128319	175044	73.30671146	26.69328854	46.61342291		
23	131785	175044	75.28678504	24.71321496	50.57357007		
24	134879	175044	77.05434062	22.94565938	54.10868125		
25	137603	175044	78.61052078	21.38947922	57.22104157		
26	140041	175044	80.00331345	19.99668655	60.00662691		26
27	142304	175044	81.29613126	18.70386874	62.59226252		27

Fig. 7: Relationship between entropy and visual quality (scanned image)

An experiment has been performed on the OBNLM filtered image given in Fig. 5 and the observations presented in Table.3. Relationship between entropy and visual quality of filtered image is given in Fig.8.

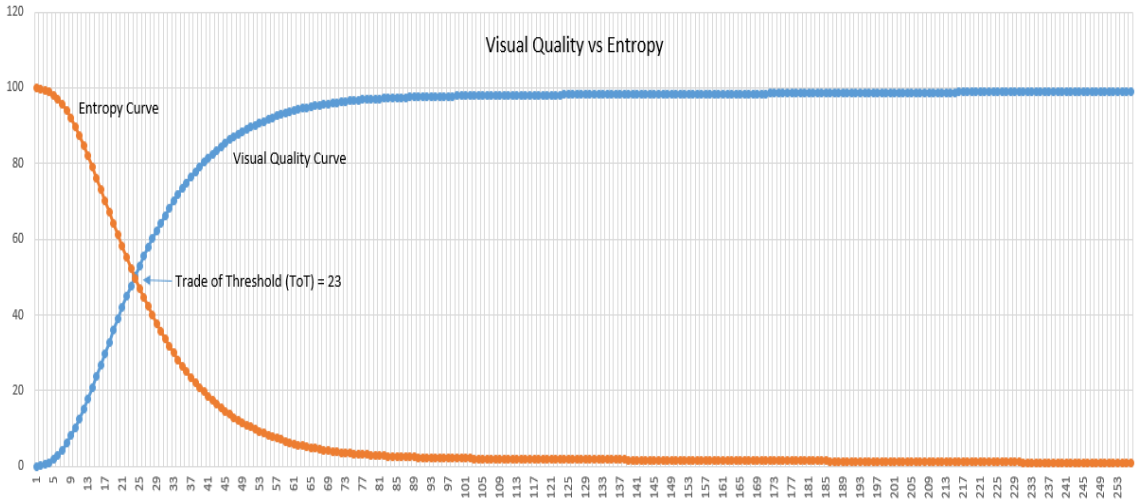

Fig. 7: Relationship between entropy and visual quality (filtered image)

Table 3: Visual quality measures of the OBNLM filtered breast image

Visual Quality, Trade of Threshold and Human Visual Quantization Threshold of ultrasonographic breast image							
Threshold	Counter	Image Size	Visual Quality	Entropy	|Entropy-Visual Quality|	ToT	HVQT
0	0	173153	0	100	100		
1	445	173153	0.256998146	99.743	99.48600371		
2	1083	173153	0.62545841	99.37454	98.74908318		
3	1843	173153	1.064376592	98.93562	97.87124682		
4	3236	173153	1.868867418	98.13113	96.26226516		
5	5180	173153	2.991573926	97.00843	94.01685215		
6	7620	173153	4.4007323	95.59927	91.1985354		
7	10522	173153	6.076706728	93.92329	87.84658654		
8	13947	173153	8.054726167	91.94527	83.89054767		
9	17689	173153	10.21582069	89.78418	79.56835862		
10	21936	173153	12.6685648	87.33144	74.66287041		
11	26312	173153	15.19580949	84.80419	69.60838103		
12	31127	173153	17.97658718	82.02341	64.04682564		
13	35932	173153	20.75158963	79.24841	58.49682073		
14	41130	173153	23.75355899	76.24644	52.49288202		
15	46317	173153	26.74917558	73.25082	46.50164883		
16	51655	173153	29.83199829	70.168	40.33600342		
17	56859	173153	32.83743279	67.16257	34.32513442		
18	62246	173153	35.94855417	64.05145	28.10289166		
19	67431	173153	38.94301571	61.05698	22.11396857		
20	72474	173153	41.85546886	58.14453	16.28906227		
21	77643	173153	44.84069003	55.15931	10.31861995		
22	82510	173153	47.65149896	52.3485	4.697002073		
23	87149	173153	50.33063245	49.66937	0.661264893	23	
24	91686	173153	52.95085849	47.04914	5.901716979		
25	96087	173153	55.49254128	44.50746	10.98508256		
26	100126	173153	57.82516041	42.17484	15.65032081		
27	104072	173153	60.10406981	39.89593	20.20813962		

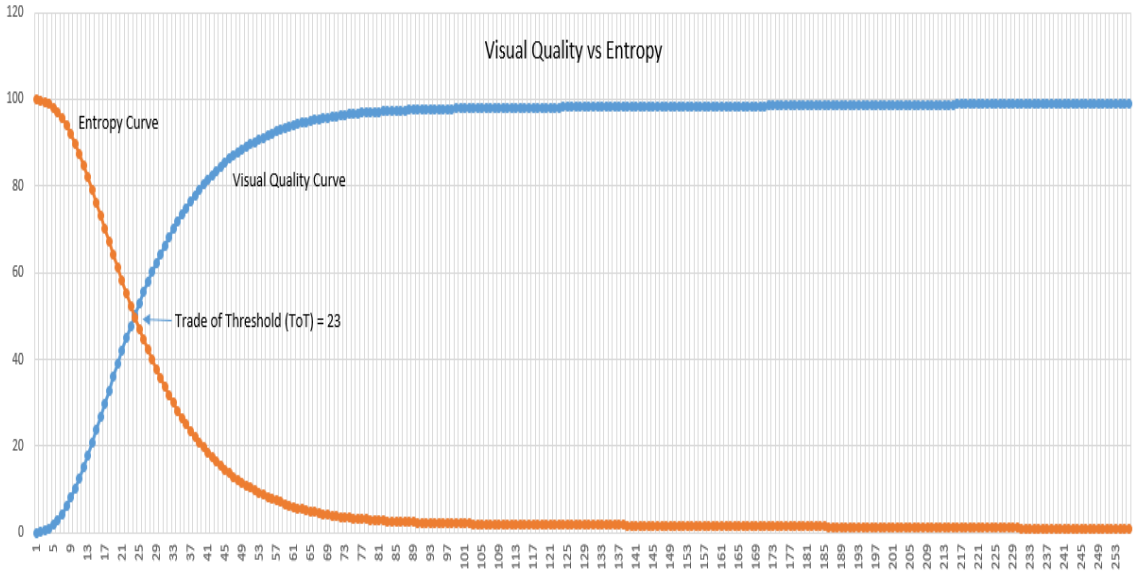

Fig. 8: Relationship between entropy and visual quality (filtered image)

Mammographic Images Gamma Correction

Gamma correction is a nonlinear operation meant for encoding and decoding intensity or tristimulus values in a still image or video.

One sample MR image with benign tumor and the other one with adenocarcinoma are considered for analysis. Gamma correction is applied on both images and results presented.

Case study #1

Image details: MR image with benign tumor

Source: Classified; Patient detail: Classified

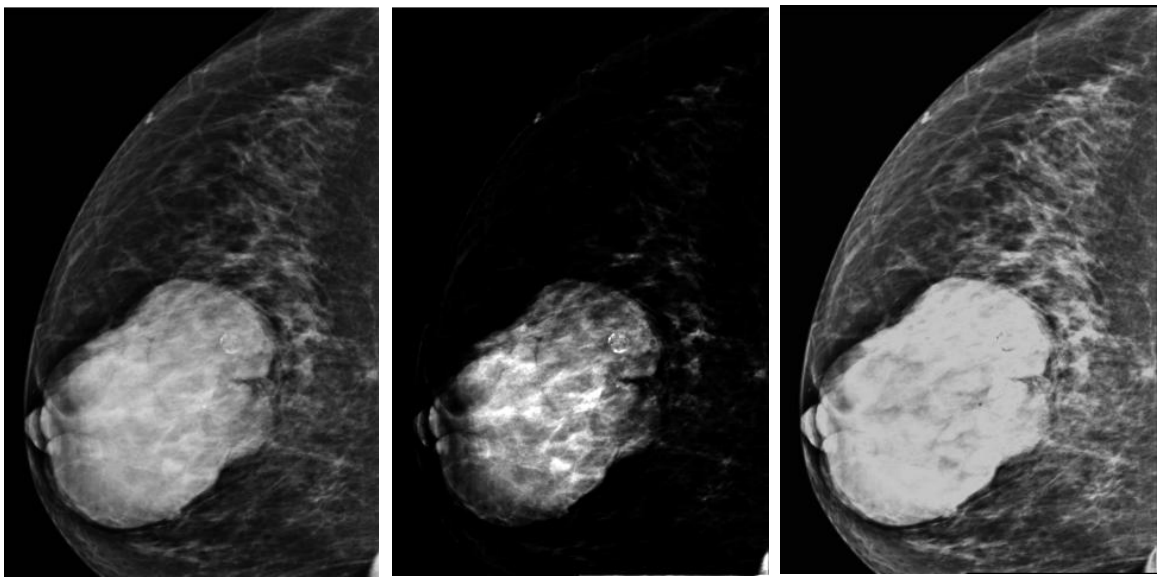

Sample MR image Benign tumor identified MR image without tumor

Fig. 9: Sample MR image with benign tumor

Statistics of the sample MR image		Statistics of gamma corrected version of the sample MR image	
Pixels Count	152160	Pixels Count	152160
Pixels without black	151752	Pixels without black	64430
Red Min	0	Red Min	0
Red Max	255	Red Max	255
Red Mean	52.4346740273396	Red Mean	23.4989747634069
Red Standard Deviation	54.141004193134	Red Standard Deviation	52.6544631887105
Red Median	35	Red Median	0
Red Total Count	152160	Red Total Count	152160
Green Min	0	Green Min	0
Green Max	255	Green Max	255
Green Mean	52.4346740273396	Green Mean	23.4989747634069
Green Standard Deviation	54.141004193134	Green Standard Deviation	52.6544631887105
Green Median	35	Green Median	0
Green Total Count	152160	Green Total Count	152160
Blue Min	0	Blue Min	0
Blue Max	255	Blue Max	255
Blue Mean	52.4346740273396	Blue Mean	23.4985410094637
Blue Standard Deviation	54.141004193134	Blue Standard Deviation	52.6543849198602
Blue Median	35	Blue Median	0
Blue Total Count	152160	Blue Total Count	152160

Visual quality of original MR image with benign tumor

Threshold	Counter	Image Size	Visual Quality	Entropy	|Entropy-Visual Quality|	ToT	HVQT
0	0	152160	0	100	100		
1	29605	152160	19.45649317	80.543507	61.08701367		
2	30441	152160	20.00591483	79.994085	59.98817035		
3	30999	152160	20.37263407	79.627366	59.25473186		
4	32563	152160	21.40049947	78.599501	57.19900105		
5	35171	152160	23.11448475	76.885515	53.77103049		
6	38935	152160	25.58819664	74.411803	48.82360673		
7	43694	152160	28.71582545	71.284175	42.56834911		
8	49156	152160	32.30546793	67.694532	35.38906414		
9	55105	152160	36.21516824	63.784832	27.56966351		
10	60989	152160	40.08215037	59.91785	19.83569926		
11	67270	152160	44.21004206	55.789958	11.57991588		
12	73378	152160	48.22423764	51.775762	3.551524711	12	
13	79235	152160	52.07347529	47.926525	4.146950578		
14	84734	152160	55.68743428	44.312566	11.37486856		
15	90004	152160	59.1508938	40.849106	18.30178759		
16	94897	152160	62.3665878	37.633412	24.7331756		
17	99258	152160	65.23264984	34.76735	30.46529968		
18	103296	152160	67.88643533	32.113565	35.77287066		
19	107086	152160	70.37723449	29.622766	40.75446898		
20	110644	152160	72.71556257	27.284437	45.43112513		
21	113781	152160	74.7772082	25.222792	49.5544164		
22	116811	152160	76.76853312	23.231467	53.53706625		
23	119614	152160	78.61067298	21.389327	57.22134595		
24	122121	152160	80.25828076	19.741719	60.51656151		24
25	124338	152160	81.71529968	18.2847	63.43059937		25
26	126397	152160	83.06848055	16.931519	66.13696109		

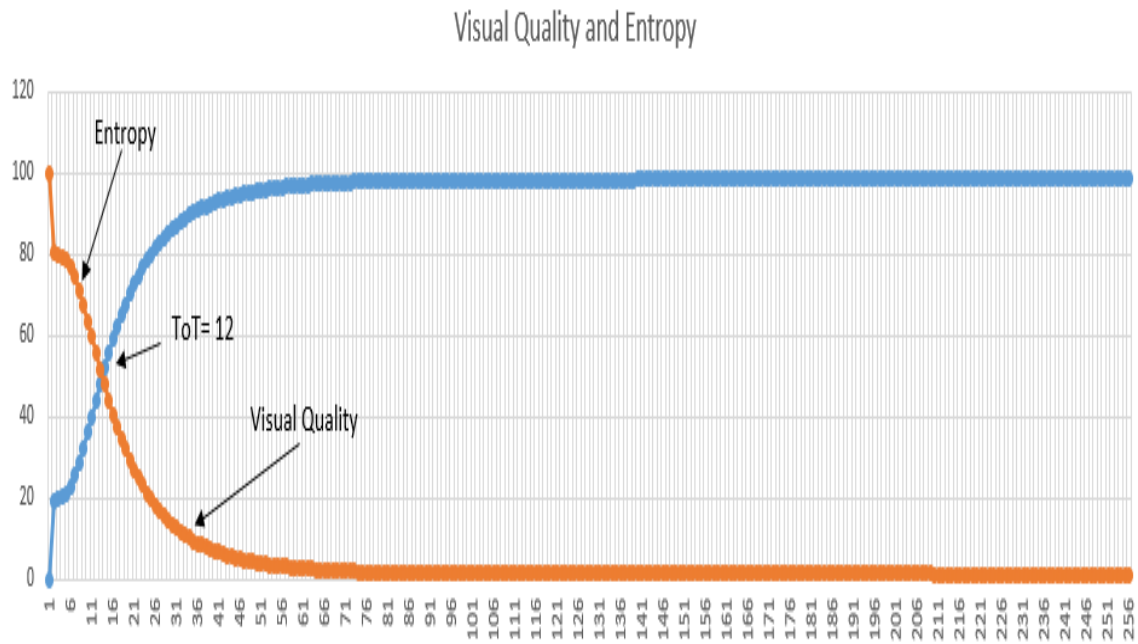

Fig. 10: Visual quality measures of original MR image with benign tumor

Visual quality of gamma corrected MR image with benign tumor

Threshold	Counter	Image Size	Visual Quality	Entropy	|Entropy-Visual Quality|	ToT	HVQT
0	0	152160	0	100	100		
1	69042	152160	45.37460568	54.6253943	9.250788644		
2	69066	152160	45.39037855	54.6096215	9.219242902	2	
3	88814	152160	58.36882229	41.6311777	16.73764458		
4	88828	152160	58.37802313	41.6219769	16.75604627		
5	99887	152160	65.64603049	34.3539695	31.29206099		
6	99887	152160	65.64603049	34.3539695	31.29206099		
7	106822	152160	70.20373291	29.7962671	40.40746583		
8	106856	152160	70.22607781	29.7739222	40.45215563		
9	111185	152160	73.07110936	26.9288906	46.14221872		
10	111204	152160	73.08359621	26.9164038	46.16719243		
11	114047	152160	74.95202419	25.0479758	49.90404837		
12	114047	152160	74.95202419	25.0479758	49.90404837		
13	116389	152160	76.49119348	23.5088065	52.98238696		
14	116417	152160	76.50959516	23.4904048	53.01919033		
15	118516	152160	77.88906414	22.1109359	55.77812829		
16	118516	152160	77.88906414	22.1109359	55.77812829		
17	120520	152160	79.20609884	20.7939012	58.41219769		
18	120538	152160	79.2179285	20.7820715	58.43585699		
19	122421	152160	80.45544164	19.5445584	60.91088328		19
20	122421	152160	80.45544164	19.5445584	60.91088328		20
21	124264	152160	81.66666667	18.3333333	63.33333333		21
22	124296	152160	81.68769716	18.3123028	63.37539432		22
23	126071	152160	82.85423239	17.1457676	65.70846477		

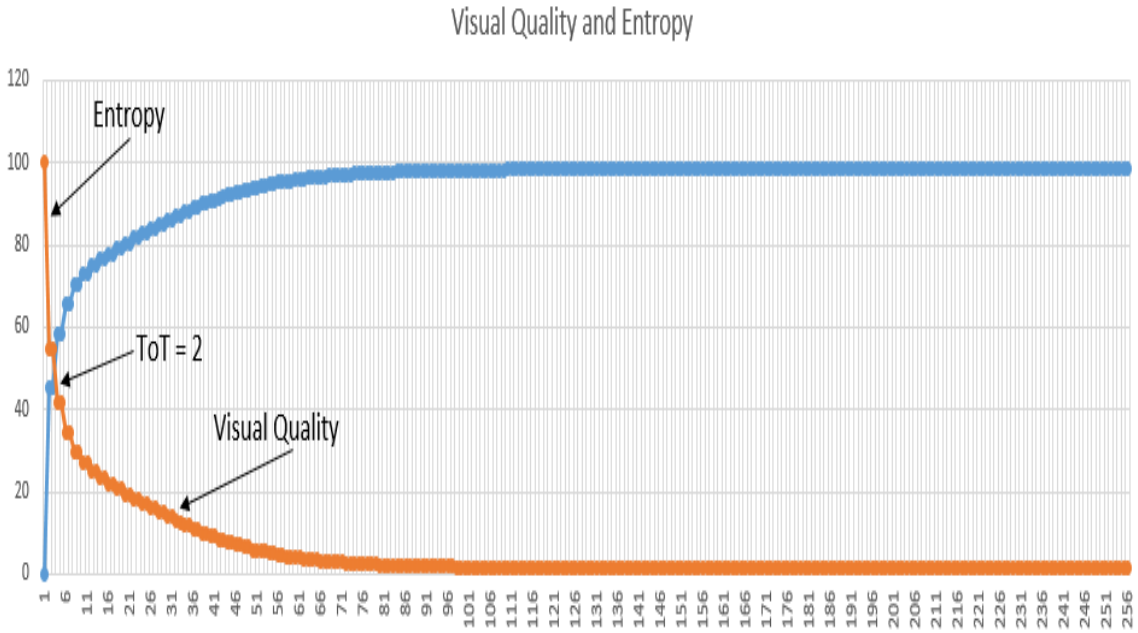

Fig. 11: Visual quality measures of gamma corrected MR image with benign tumor

Results &Observations

- Breast cancer can be identified with ultrasonography scanners by radiologists.
- Speckle noise is difficult to remove if the image is blended with different speckle noise.
- Speckle noise can be removed with different kinds of filters
- For reducing speckle noise the best procedure is LN-OBNLM
- Better visual quality and considerable entropy can be obtained after filtering.
- In the gamma corrected image, the medians of Red, Green and Blue components are reduced to '0' from the original values
- The medians of Red, Green and Blue white balanced components are reduced to almost one third of their original values in the gamma corrected image.
- Trade of Threshold (ToT) value is reduced to 2 in the gamma corrected image from the value of 12 of original image, which means improvement in the visual quality.

Conclusion

All said and done, current practice in cancer studies makes use of images obtained from advanced scanners like x-ray tomography, mammography, MRI, PET, SPECT to name a few. Images obtained using such advanced scanning systems do exhibit better visual quality and entropy for in-depth image analysis.

References

1. *Blakely T, Shaw C, Atkinson J, Cunningham R, Sarfati D. Social inequalities or inequities in cancer incidence? Repeated census-cancer cohort studies, New Zealand 1981-1986 to 2001-2004. Cancer Causes Control. 2011 Sep;22(9):1307–18. doi: 10.1007/s10552-011-9804-x.*
2. *Smigal C, Jemal A, Ward E, Cokkinides V, Smith R, Howe HL, Thun M. Trends in breast cancer by race and ethnicity: update 2006. CA Cancer J Clin. 2006;56(3):168–83. doi: 10.3322/canjclin.56.3.168. https://onlinelibrary.wiley.com/resolve/openurl?genre=article&sid=nlm:pubmed&issn=0007-9235&date=2006&volume=56&issue=3&spage=168.*
3. *Ponraj DN, Jenifer ME, Poongodi DP, Manoharan JS. A survey on the preprocessing techniques of mammogram for the detection of breast cancer. J Emerging Trends Computer Info Sci. 2011;2(12)*
4. *Rangayyan RM, Ayres FJ, Leo Desautels JE. A review of computer-aided diagnosis of breast cancer: toward the detection of subtle signs. J Franklin Inst. 2007 May;344(3-4):312–48. doi: 10.1016/j.jfranklin.2006.09.003.*
5. *Ganesan K, Acharya UR, Chua KC, Min LC, Abraham KT. Pectoral muscle segmentation: a review. Comput Methods Programs Biomed. 2013 Apr;110(1):48–57. doi: 10.1016/j.cmpb.2012.10.020.*
6. *Ge M, Mainprize JG, Mawdsley GE, Yaffe MJ. Segmenting pectoralis muscle on digital mammograms by a Markov random field-maximum a posteriori model. J Med Imaging (Bellingham) 2014 Oct;1(3):34503. doi: 10.1117/1.JMI.1.3.034503. http://europepmc.org/ abstract/MED/26158068.*
7. *Ali MA, Czene K, Eriksson L, Hall P, Humphreys K. Breast tissue organisation and its association with breast cancer risk. Breast Cancer Res. 2017 Sep 6;19(1):103. doi: 10.1186/s13058-017-0894-6. https://breast-cancer-research.biomedcentral.com/articles/ 10.1186/s13058-017-0894-6.*
8. *Eltoukhy MM, Faye I. An Adaptive Threshold Method for Mass Detection in Mammographic Images. Proceedings of the International Conference on Signal and Image Processing Applications; IEEE'13; Oct. 8-10, 2013; Melaka, Malaysia. 2013. pp. 374–378.*
9. *Shih FY. Image Processing and Pattern Recognition: Fundamentals and Techniques. USA: Wiley-IEEE Press; 2010.*
10. *Biltawi M, Al-Najdawi N, Tedmori S. Mammogram Enhancement and Segmentation Methods: Classification, Analysis, and Evaluation. Proceedings of the 13th International Arab Conference on Information Technology; ACIT'12; December 10-13, 2012; Jordan, Zarq. 2012. pp. 477–85.*
11. *de Oliveira HC, Mencattini A, Casti P, Martinelli E, di Natale C, Catani JH, de Barros N, Melo CF, Gonzaga A, Vieira MA. Reduction of False-Positives in a CAD Scheme for Automated Detection of Architectural Distortion in Digital Mammography. Proceeding of the Conference on Computer-Aided Diagnosis; SPIE'18; February 10-15, 2018; Houston, Texas, United States. 2018. p. 105752P.*
12. *Liu X, Zeng Z. A new automatic mass detection method for breast cancer with false positive reduction. Neurocomputing. 2015 Mar;152:388–402. doi: 10.1016/ j.neucom.2014.10.040. doi: 10.1016/j.neucom.2014.10.040.*
13. *Jen CC, Yu SS. Automatic detection of abnormal mammograms in mammographic images. Expert Syst Appl. 2015 Apr;42(6):3048–55. doi: 10.1016/j.eswa.2014.11.061.*
14. *Ayer T, Chen Q, Burnside ES. Artificial neural networks in mammography interpretation and diagnostic decision making. Comput Math Methods Med. 2013;2013:832509. doi: 10.1155/2013/832509. doi: 10.1155/2013/832509.*
15. *Magna G, Casti P, Jayaraman SV, Salmeri M, Mencattini A, Martinelli E, Natale CD. Identification of mammography anomalies for breast cancer detection by an ensemble*

of classification models based on artificial immune system. Knowl Based Syst. 2016 Jun;101:60–70. doi: 10.1016/j.knosys.2016.02.019.

16. *Wang H, Zheng B, Yoon SW, Ko HS. A support vector machine-based ensemble algorithm for breast cancer diagnosis. Eur J Oper Res. 2018 Jun;267(2):687–99. doi: 10.1016/j.ejor.2017.12.001. doi: 10.1016/j.ejor.2017.12.001.*
17. *Singh B, Jain V, Singh S. Mammogram mass classification using support vector machine with texture, shape features and hierarchical centroid method. J Med Imaging & Health Infor. 2014 Oct 1;4(5):687–96. doi: 10.1166/jmihi.2014.1312. doi: 10.1166/jmihi. 2014.1312.*
18. *Sonar P, Bhosle U, Choudhury C. Mammography Classification Using Modified Hybrid SVM-KNN. Proceedings of the International Conference on Signal Processing and Communication; IEEE'17; July 28-29, 2017; Coimbatore, India. 2017. pp. 305–11.*
19. *Gardezi SJ, Faye I, Eltoukhy MM. Analysis of Mammogram Images Based on Texture Features of Curvelet Sub-Bands. Proceedings of the 5th International Conference on Graphic and Image Processing; SPIE'14; January 10, 2014; Hong Kong. 2014. p. 906924.*
20. *Pratiwi M, Alexander. Harefa J, Nanda S. Mammograms classification using gray-level co-occurrence matrix and radial basis function neural network. Procedia Comput Sci. 2015;59:83–91. doi: 10.1016/j.procs.2015.07.340. doi: 10.1016/j.procs.2015.07.340.*